

A FREE-SPACE METHOD FOR COMPLEX PERMITTIVITY MEASUREMENT OF BULK AND THIN FILM DIELECTRICS AT MICROWAVE FREQUENCIES

Zaiki Awang*, Fatimah A. M. Zaki, Noor H. Baba, Ahmad S. Zoolfakar, and Raudah A. Bakar

Microwave Technology Centre, Universiti Teknologi MARA, Shah Alam 40450, Malaysia

Abstract—A free-space, non-destructive method for measuring the complex permittivity of a double-layer bulk dielectrics and thin film oxide layers at microwave frequencies have been developed. The method utilizes a spot-focusing antenna system in conjunction with a vector network analyzer in the range of 18–26 GHz. The bulk dielectric was measured using the Transmission Method and Metal-Backed Method, while the Metal-Backed Method was used to investigate the thin films. Both types of samples were sandwiched between two quarter-wavelength Teflon plates to improve the mismatch at the frequencies of measurement. The thin film sample arrangement was backed by an additional metal plate. The double-layer bulk dielectric samples were Teflon-PVC and Plexiglas-PVC, while the thin film samples consisted of SiO₂ layers of different thicknesses grown on doped and undoped Si wafer substrates. The relative permittivity obtained for PVC ranged between 2.62 to 2.93, while those for Plexiglas exhibited values between 2.45 to 2.63. The relative permittivity of SiO₂ deposited on these wafers was between 3.5 to 4.5. All these values are in good agreement with published data. The advantage of the method is its ability to measure the dielectric properties of the films at the mid-frequency band irrespective of the substrate type used. Simulations of the measurement setup were carried out using *CST Microwave Studio* and the simulation results agreed closely with the measurements.

Received 15 March 2013, Accepted 29 April 2013, Scheduled 6 May 2013

* Corresponding author: Zaiki Awang (zaiki.awang@gmail.com).

1. INTRODUCTION

The gate dielectric is an important element of a CMOS transistor since the conducting channel between the source and the drain is formed underneath the gate. As such it plays an important role in transistor switch speed, power consumption efficiency, and device reliability [1].

Silicon dioxide (SiO_2) has been used over forty years as the passivation layer and gate dielectric of choice because of its favourable physical and chemical properties, including thermodynamic stability, as well as being a native oxide of silicon yielding a stable Si/ SiO_2 interface [2].

Semiconductors can be oxidized by various methods. These include thermal oxidation, electrochemical anodization and plasma-enhanced chemical vapor deposition (PECVD). The ability silicon to form a dioxide passivation layer is one of the key enabling factors in silicon technology. SiO_2 layers are formed on bare silicon surfaces at elevated temperatures in the presence of an oxidant. The process is called thermal oxidation. The gate oxides are generally grown by a thermal oxidation process as it is the only method that can provide the highest quality oxides having the lowest interface trap densities [1]. Growing thick oxide layers require longer oxidation times when the oxidizing gas used is dry oxygen. To achieve faster oxidations, water vapor (which, at the oxidation temperatures is in the form of steam) is used, and the process is called *steam oxidation* or *wet oxidation*.

Over the years, the silicon industry has been scaling SiO_2 for low power, high performance CMOS logic applications by reducing the dielectric thickness [2]. To achieve this, different approaches of growing thin oxides of silicon can be employed — this has included reducing the oxide growth temperature, diluting the oxidant gas with nitrogen, and reducing the oxidant gas temperature [2].

Equally important is the ability of a deposition technique that can guarantee the electrical properties of the oxide films are both reproducible and reliable. To this end, it is therefore pertinent that a reliable method of measuring the electrical properties of these films is developed. More importantly for the semiconductor industry, the method should not introduce damage to the film being measured so that the electrical properties being investigated are not affected. Recently, a non-contacting free-space technique of measuring the electromagnetic properties of dielectric materials has been developed using microwave non-destructive testing (MNMT) [3]. This method has been expanded to the characterization of SiO_2 gate dielectric films used in semiconductors, and detailed results are reported herewith. To our knowledge, MNMT has not been exclusively applied to measure

the physical properties of double-layer dielectrics prior to this, and this paper presents a comprehensive report of such attempt.

2. THEORY

MNDT is a contactless, non-destructive technique and requires no sample preparation. The method is fast, accurate and convenient for measuring complex permittivity and complex permeability of a material. Two MNDT methods, namely transmission method and metal-backed method are commonly used to measure the dielectric properties of a material. In this work, the two methods were improvised and developed for application to double-layer bulk dielectrics and thin film oxides. To verify the accuracy of these methods, standard reference materials PVC-Plexiglas, Plexiglas-PVC, and Teflon-PVC have been tested.

At microwave frequencies, electromagnetic signals are reflected by metallic surfaces, but they can penetrate most dielectrics. This feature makes it well suited for inspecting dielectric materials and composite structures in many applications [4]. In this work, the metal-backed method is used to measure the forward reflection coefficient S_{11} of epitaxial oxide layers of various thicknesses on a Si substrate. The sample is sandwiched with two quarter-wavelength transformers constructed of Teflon plates for impedance matching, and the whole structure is backed by a metal plate.

2.1. Transmission Method (TM)

The assembly of TM was originally proposed by Ghodgaonkar et al. [5], and featured one sample sandwiched between two quarter-wave transformers. Owing to the symmetry of the assembly, in this case, which gives rise to reciprocity, $S_{11} = S_{22}$ and $S_{12} = S_{21}$ [4]. Hence, only the free-space input reflection and forward transmission coefficients, S_{11} and S_{21} , need to be measured.

In our work, the sample is a double-layered dielectric, and the impedance transformers consisted of two Teflon plates a quarter wavelength thick at mid-band.

For layered samples, the S_{11} of the Teflon-Sample 1-Sample 2-Teflon assembly is not equal to S_{22} [5]. Hence, the output reflection coefficient, S_{22} was also measured. The reflection and transmission coefficients S_{11} and S_{21} of the double-layer sample are calculated from measured S_{11}^m and S_{21}^m of the assembly by substituting the permittivity and thickness of Teflon plates. In this case, the $ABCD$ matrix of the

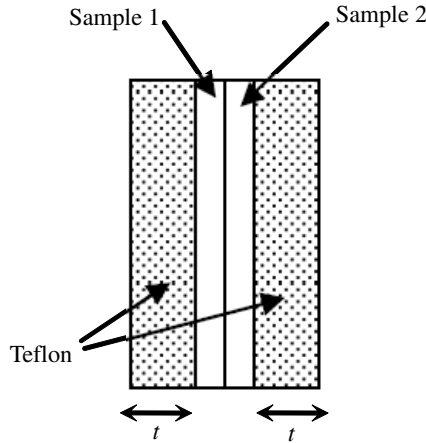


Figure 1. Schematic diagram of Teflon-Sample 1-Sample 2-Teflon assembly.

assembly is given by [5];

$$\begin{aligned}
 [A^m] &= \begin{bmatrix} A^m & B^m \\ C^m & D^m \end{bmatrix} \\
 &= \frac{1}{2S_{21}} \begin{bmatrix} (1+S_{11})(1-S_{22})+S_{21}^2 & (1+S_{11})(1+S_{22})-S_{21}^2 \\ (1-S_{11})(1-S_{22})-S_{21}^2 & (1-S_{11})(1+S_{22})+S_{21}^2 \end{bmatrix} \quad (1)
 \end{aligned}$$

As the permittivity and thickness of the Teflon are known, the $ABCD$ matrix of Teflon plates is as follows

$$[A_T] = \begin{bmatrix} \cosh(\gamma_T t) & Z_T \sinh(\gamma_T t) \\ \frac{1}{Z_T} \sinh(\gamma_T t) & \cosh(\gamma_T t) \end{bmatrix} \quad (2)$$

where $\gamma_T = j \frac{2\pi\sqrt{\epsilon_T}}{\lambda_o}$ is the propagation constant in Teflon t and ϵ_T is the thickness and relative permittivity of Teflon respectively, and λ_o is the free-space wavelength. Z_T is the normalized characteristic impedance of the Teflon plates, which is related to its permittivity and permeability by the following expression

$$Z_T = \sqrt{\frac{\mu_o \mu_T}{\epsilon_o \epsilon_T}} \quad (3)$$

where ϵ_o and μ_o is the permittivity and permeability of free space respectively. For a non-magnetic medium $\mu_T = 1$, thus (3) becomes

$$Z_T = \sqrt{\frac{\mu_o}{\epsilon_o \epsilon_T}} = \sqrt{\frac{\mu_o}{\epsilon_o}} \frac{1}{\sqrt{\epsilon_T}} \quad (4)$$

Substituting $Z_o = \sqrt{\frac{\mu_o}{\epsilon_o}}$ into (4) reduces the expression to

$$Z_T = Z_o \frac{1}{\sqrt{\epsilon_T}} \tag{5}$$

Dividing (5) by Z_o yields the normalized characteristic impedance of Teflon

$$Z_{TN} = \frac{1}{\sqrt{\epsilon_T}} \tag{6}$$

The $ABCD$ matrix of the double-layer dielectric sample is denoted by $[A_S]$, where $[A_S] = [A_{\text{Sample1}}] \cdot [A_{\text{Sample2}}]$, and the relationship between $[A^m]$ and $[A_S]$ is given by the following matrix expression:

$$[A_S] = [A^T]^{-1} \cdot [A^m] \cdot [A^T]^{-1} \tag{7}$$

The parameters S_{11} and S_{21} of Sample 2 can be obtained using the following standard relations [6]:

$$S_{11} = \left[\frac{A + B - C - D}{A + B + C + D} \right] \quad S_{21} = \left[\frac{2}{A + B + C + D} \right] \tag{8}$$

After removing the effects of the Teflon plates and that of Sample 1, the system can be analyzed as a planar sample of thickness d placed in free-space. The calculated S_{21}^c values can be obtained using (8) above, which, if expressed in terms of the reflection coefficient Γ and transmission coefficient T takes the form [6]:

$$S_{21}^c = T \frac{(1 - \Gamma^2)}{(1 - \Gamma^2 T^2)} \tag{9}$$

Γ is the reflection coefficient of the air-Sample interface and is given as

$$\Gamma = \frac{Z_{SN} - 1}{Z_{SN} + 1} \tag{10}$$

while T is the transmission coefficient given by

$$T = e^{-\gamma d} \tag{11}$$

Z_{SN} and γ are the normalized characteristic impedance and propagation constant of the sample, and are similarly related to the permittivity of the sample ϵ_s by (6), *viz.*

$$Z_{SN} = \frac{1}{\sqrt{\epsilon_s}} \tag{12}$$

$$\gamma = \gamma_o \sqrt{\epsilon_s} \tag{13}$$

Here $\gamma_o = \frac{j2\pi}{\lambda_o}$. Using Equations (5) to (9), we can therefore find S_{21}^c in terms of ϵ . However, ϵ cannot be expressed explicitly in terms of

S_{21}^c . Therefore, it is necessary to determine ε iteratively by assuming a guess value for the sample. This is done by using a zero finding technique which finds the zeros of the error function, which is defined as the difference between the measured and calculated S_{21} values,

$$E = |S_{21}^m - S_{21}^c| \quad (14)$$

2.2. Metal-Backed Method (MBM)

The assembly of MBM discussed by Ghodgaonkar et al. [7] has a perfectly conducting plate inserted behind an unknown one-layer sample. The S_{11} was measured and related to the normalized wave impedance in the unknown material. In our work, however, the sample is a double-layered dielectric sandwiched between two Teflon quarter-wave transformers, backed by a metal plate. Fig. 2 illustrates the said assembly.

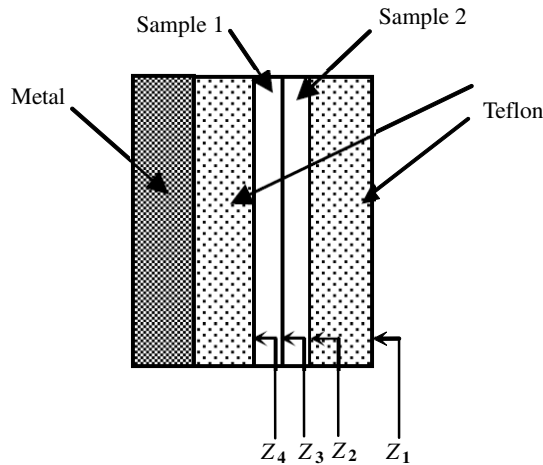


Figure 2. Schematic diagram of metal-backed method set-up.

For this method, the complex permittivity of the sample will be calculated from measured reflection coefficient S_{11}^m . t is the thickness of Teflon plates, while d_1 and d_2 are thicknesses of Samples 1 and 2 respectively. The characteristic impedances of Samples 1 and 2 are similarly given by (6) previously, by substituting the permittivity of Teflon with those of the samples. The permittivity of Teflon was determined from our own measurements, the experimental set-up of which was based on the original effort by [7]. Details of these experiments have been reported elsewhere [3, 8].

From transmission line theory it can be shown that the input impedance of the assembly is

$$Z_1 = Z_T \frac{Z_2 + jZ_T \tan \beta_T t}{Z_T + jZ_2 \tan \beta_T t} \tag{15}$$

where β_T is the phase constant of Teflon given by

$$\beta_T = \frac{2\pi\sqrt{\epsilon_T}}{\lambda_0} \tag{16}$$

The calculated S_{11}^c can be written as follows

$$S_{11}^c = \frac{Z_1 - 377}{Z_1 + 377} \tag{17}$$

The error function E takes the same form as (14), by replacing S_{21}^c with S_{11}^c . Further, S_{21}^c is obtained using (15) and (16), with the characteristic impedances of Samples 1 and 2 calculated using (6) previously. The relative permittivity of the sample ϵ_S is again determined by finding the zeros of the error function.

3. MEASUREMENT SETUP

The measurement setup is shown in Fig. 3. The experiment was carried out over a frequency range of 18–26 GHz. Two spot-focusing horn lens antennas are mounted back-to-back 610 mm apart on a large table. The antennas are connected to the two ports of a *Wiltron 37269B* VNA using circular-to-rectangular waveguide adapters, rectangular waveguide to coaxial line adapters, and precision coaxial cables. *Millitech* series WAC circular-to-rectangular waveguide adapters were used to provide transition from standard rectangular waveguide to circular waveguide [9]. The antennas are Gaussian optics lens antennas manufactured by *Millitech Inc.* The diameter of the lens and the housing length of the antennas were 304.8 mm each. In Gaussian optics

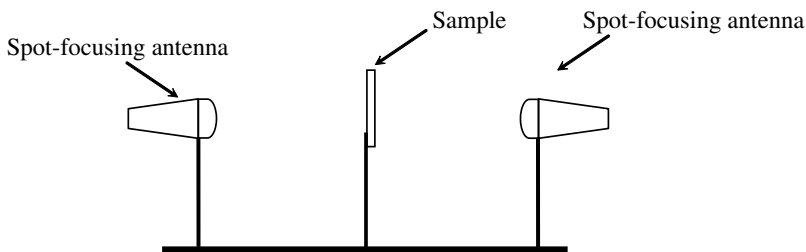


Figure 3. Schematic diagram of the measurement set-up.

transmission, the propagating signal is not confined by metal or by dielectric walls, but travels in free space, resulting in a very low loss system. The ratio of the focal distance to antenna diameter (F/D) of the lens is equal to one and D is approximately 30.5 cm. A lens antenna with its beam focused at a finite distance (typically a few lens diameters' length in front of the lens) can be configured for applications requiring a spot beam focus [9].

A personal computer is used for FORTRAN programming. Errors in free-space measurement of S -parameters due to multiple reflections between the antennas and the mode transitions are eliminated by implementing LRL (Line, Reflect, Line) calibration techniques in free-space [4, 10]. Post calibration errors are minimized by using the time-domain gating feature of the VNA.

A specially fabricated sample holder is mounted at the common focal plane for holding planar samples. The transmit and receive horns were mounted on a carriage and the distance between them can be changed with an accuracy of 0.001 in. using a dial indicator. Because of spot-focusing lens antennas, diffraction effects at the edges of the sample are negligible if the minimum transverse dimension of the sample is greater than three times the beamwidth of the antenna at the focus [5].

In this work, a quarter-wavelength transformer was implemented for impedance matching. Teflon was used as a matching layer to reduce the reflectivity of the SiO_2 . As the measurements were done at 18 to 26 GHz, the matching occurs at a mid-band frequency of 22 GHz. The thickness of Teflon matching layer is 2.35 mm. The samples used were SiO_2 grown on various doped and undoped Si substrates. The network analyzer measures the amplitude and phase of reflected and transmitted signals in the free-space and is capable of making accurate measurement from 40 MHz to 40 GHz frequency range. The permittivity of the samples was calculated based on the measured S_{11} values. For comparison, a full three-dimensional electromagnetic simulation was carried out using an industry-standard electromagnetic simulator *CST Microwave Studio*.

4. EXPERIMENTAL RESULTS AND DISCUSSIONS

4.1. Double-Layer Bulk Dielectrics

In this work, the double-layer bulk dielectric samples were arranged as Sample 1-Sample 2. Two sets of samples were used, one each for transmission and metal-backed methods. For the transmission method, the samples used were Plexiglas-PVC and PVC-Plexiglas, while Plexiglas-PVC and Teflon-PVC were used in the metal-back

procedure. The thicknesses of the samples are 5.8 mm (Plexiglas) and 3.0 mm (Teflon and PVC). In order to reduce the measurement errors, the sample thickness was required to be close to odd multiples of quarter wavelength [7]. This therefore limits the frequency range over which the samples can be measured.

In the transmission method arrangement, and in accordance with Equations (7) to (9), the unknown dielectric is denoted as Sample 2. For the PVC-Plexiglas combination for example, the unknown is the Plexiglas, and thus the measured values were those of Plexiglas. The measured ϵ' values are plotted in Fig. 4 above for Plexiglas (green trace) and PVC (red) respectively. Using the transmission method, the relative permittivity for PVC was found to be between 2.65 to 2.93, and for Plexiglas between 2.45 to 2.63. The mean values for PVC and Plexiglas were 2.81 and 2.55 respectively — these compare favourably with those reported in the literature (2.81 against 2.9 for PVC [7], and 2.55 against 2.59 for Plexiglas [10]). From the graph it can be seen that both sets exhibit an almost similar trend for frequencies lower than about 24 GHz, but the trend differ slightly beyond that, with the Plexiglas showing an upward trend in contrast to PVC. The decrease in ϵ' for PVC could be attributed to the quality of the samples used, which could have been caused by manufacturing. The fluctuation of the values above 22 GHz may have been caused by errors of the measured S_{11} , S_{21} , and S_{22} and air gap that could have existed in the sample assembly. Nevertheless, these fluctuations are of the order of 3 to 4% only, and can therefore be considered small. The fact that these fluctuations are small, and that the measured values compare very well with those reported in the literature imply that this method is capable of yielding acceptable accuracies in real applications.

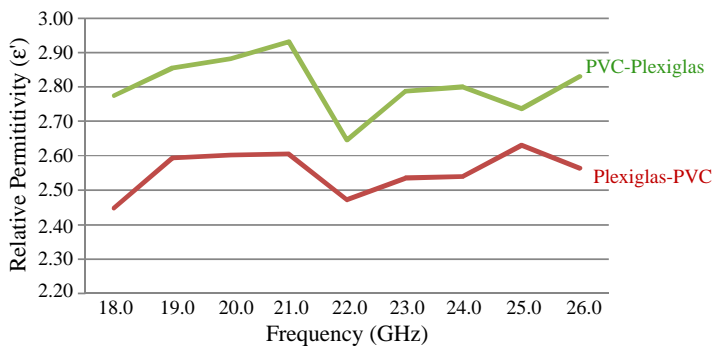


Figure 4. Measured relative permittivity values using the transmission method.

Figure 5 shows the plot of measured ϵ' obtained from the metal-backed method. With the metal-backed method, the measured values of ϵ' for Plexiglas-PVC were between 2.26 to 3.09, and between 2.60 to 2.93 for Teflon-PVC. The mean values are 2.98 and 2.73 respectively, which agree well with the published value of 2.9 [7].

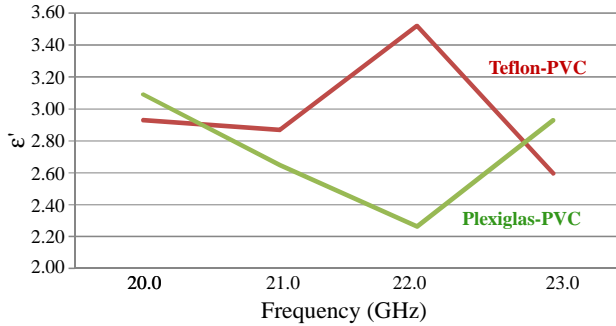


Figure 5. Measured relative permittivity values using the metal-backed method.

4.2. Thin Film Dielectric

Figures 6 and 7 show the magnitudes of the forward reflection coefficient, S_{11} , for SiO_2 deposited on p- and n-type Si substrates respectively. In Fig. 6 a minimum of $|S_{11}|$ is seen at 21 to 24 GHz, showing that the sample is matched due to the effect of the quarter-wave impedance transformer, resulting in least reflection.

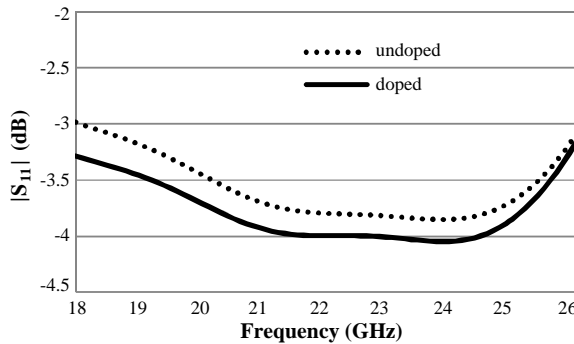


Figure 6. Measured $|S_{11}|$ for SiO_2 deposited on undoped and p-type Si substrates.

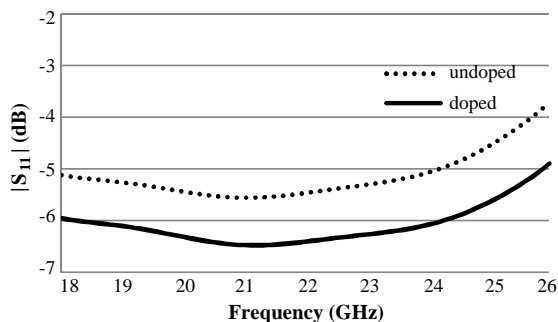


Figure 7. Measured $|S_{11}|$ for SiO_2 deposited on undoped and n-type Si substrates.

The differences in $|S_{11}|$ seen for the oxide layers grown on doped and undoped substrates show the effect of doping on the Si substrates. In this experiment, the n-type wafer was doped with phosphorus making it electron-rich, while the p-type wafer was doped with boron which makes it hole-rich. The differences in the S_{11} values between doped and undoped substrates are thus due to the resistivity of the Si.

The oxidation of the Si surface affects the final distribution of the dopants, which are related to the relocation of the top level dopants after the oxidation. For n-type doping, a pile-up effect occurs. As the oxide-silicon interface advances into the surface, the n-type dopant atoms segregate into the Si rather than the oxide [11]. This results in the piling up of n-type dopants in the Si-SiO₂ wafer surface and the number of dopants increases, hence changing the electrical performance of the dielectric. Meanwhile, for p-type doping, the opposite occurs as boron atoms are more soluble in oxide and are therefore drawn up into it [11]. This lowers the concentration of boron atoms, which lowers the surface concentration and also affects the electrical performance of the dielectric layer.

The experimental results can also be explained in terms of conductivity of a semiconductor which is given as

$$\sigma = en\mu_e + ep\mu_h \quad (18)$$

where n and p are the electron and hole concentrations in the conduction band and valence band respectively, and μ_e and μ_h are their respective mobilities. Fig. 8 compares the $|S_{11}|$ of SiO_2 grown on both n- and p-type Si wafers. It is shown that samples grown on n-type Si had lower $|S_{11}|$ than those on p-type — this is due to the higher conductivity of n-type Si due to the higher mobility of electrons compared to holes. In a p-type material, there are more

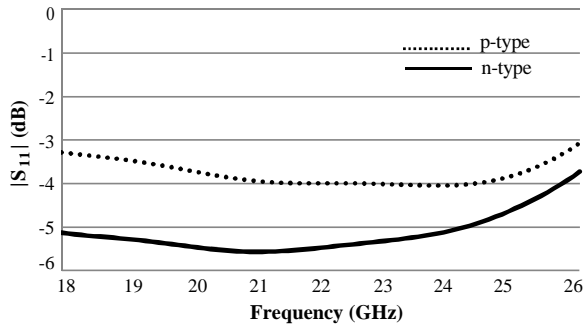


Figure 8. $|S_{11}|$ of SiO_2 films grown on n- and p-type Si substrates.

holes than electrons for electrical conduction since the negatively charged boron atoms are immobile and hence cannot contribute to the conductivity [12]. It can be concluded that the reason for a higher resistance with p-type doping compared with the same amount of n-type doping is that $\mu_h \ll \mu_e$.

The magnitude and phase values of S_{11} were then inserted into a computer program to calculate the relative permittivity. Fig. 9 depicts these values of all the four SiO_2 samples. From the graph, it can be seen that the permittivity for all samples vary from 2.0 to 5.7, and increases as the frequency increases. However, the traces intersect at 22 GHz with a common value near 3.8. This shows that the method is able to differentiate the oxide layer from the substrate at the mid-band, irrespective of the substrate type. The permittivity values found in our method compare favourably to the one reported by Kawate and Prijamboedi [13]. The relative permittivity values at 22 GHz for oxides grown on different substrate types are shown in Table 1.

Table 1. Electrical properties at 22 GHz for SiO_2 grown on different doped and undoped substrates.

Substrate type	$ S_{11} $	ϵ_r	$\tan \delta$	Resistivity ($\Omega \cdot \text{m}$)
Undoped	0.633	3.82	0.29	0.013
p-type	0.631	3.73	0.23	0.017
n-type	0.594	3.8	0.16	0.024

Figure 10 depicts the imaginary part of the relative permittivity (ϵ'') values of SiO_2 . The values vary for different types of substrates. Oxide films deposited on n-type Si substrates exhibited the lowest ϵ'' of about 35, while the undoped substrates showed values around 63.

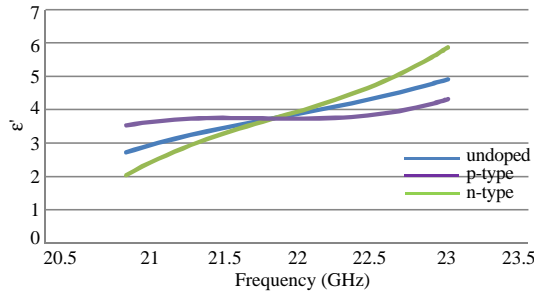


Figure 9. Relative permittivity versus frequency for SiO₂ samples grown on various substrates.

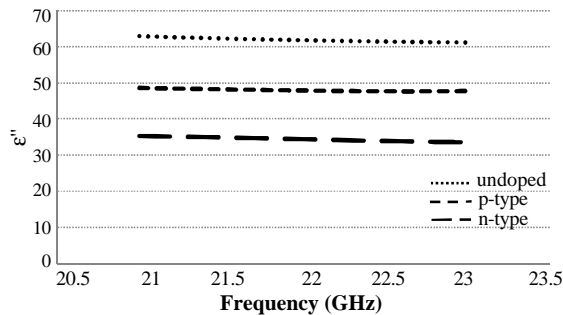


Figure 10. ϵ'' versus frequency for SiO₂ samples grown on various substrates.

These ϵ'' values correspond to $\tan \delta$ of between 0.16 to 0.3. These values are higher than those reported for SiO₂ by other workers using different methods [14, 15] but they are reflective of the film quality of the samples tested, not the inaccuracy of the method employed.

Using ϵ'' we can determine the conductivity (and hence resistivity) of the oxide films using

$$\sigma = 2\pi f \epsilon_o \epsilon'' \tag{19}$$

The resistivity values are tabulated in Table 1. Again we see that the film resistivity are almost unaffected by the underlying substrate type, as expected. The values are lower than those reported by others [15] but the poor resistivity exhibited by the oxide films is again indicative of the quality of oxidation method used in our experiment. ϵ'' represents the energy losses due to polarization and conduction, the value thus reflects the material defects. The material used by Baker-Jarvis et al. [16] was fused silica, which is a bulk material, and is known to have better dielectric characteristics than thin film.

4.2.1. Comparison with Simulation

For comparison, computer simulations were carried out using *CST Microwave Studio*. The conductivity values were varied to curve-fit the simulated results with experimental data as illustrated in Fig. 11. The best fit occurs when the conductivity is 60 S/m, which is close to the values obtained from measurements of between 42 S/m to 77 S/m calculated from the resistivity values of Table 1. The graph of Fig. 11 also indicates a minimum at approximately 22 GHz, where matching occurred due to the presence of the quarter-wave impedance transformer. The measurement results were then compared to the simulation — an example is shown in Fig. 12 for samples grown on p-type Si substrates. The graph shows a good agreement between measurement and simulation.

The magnitude and phase of S_{11} were then inserted into the computer program to calculate ϵ_r — the values are plotted in Fig. 13. The ϵ_r values decreased with frequency in agreement with theory. The

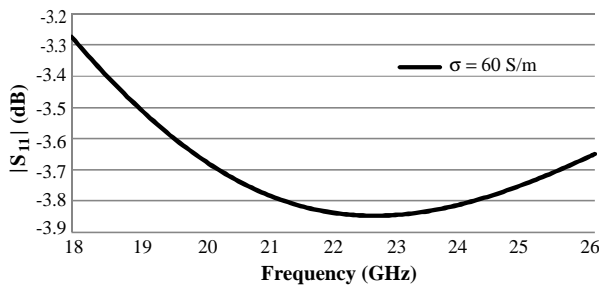


Figure 11. Simulated $|S_{11}|$ for SiO_2 grown on p-type Si substrates with $\sigma = 60 \text{ S/m}$.

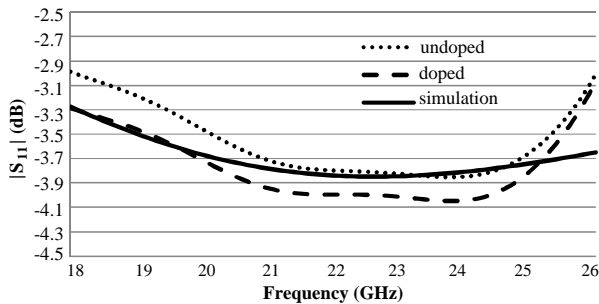


Figure 12. Comparison of experimental and simulated results for oxide layers grown on p-type wafers.

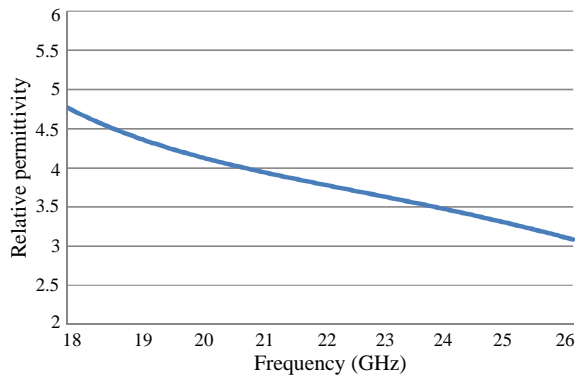


Figure 13. Simulated ϵ_r values against frequency.

simulation results give ϵ_r values between 3.2 and 4.7. These compare favourably to those reported by Kawate and Prijamboedi [13] and others [17, 18], who obtained values ranging between 3.5 to 4.5.

Figure 14 shows the simulated and measured relative permittivity of SiO_2 layers grown on p-type Si. It can be seen that the simulation results agree quite well with measurement, although the simulated values are more constant compared to measurement. This might be due to errors which arose from sample processing conditions. These include crystal defects which give rise to uneven SiO_2 growth, poor film deposition, and variations of doping across the active layers of the wafer [11]. The quality of the oxide layer is influenced by the presence of defects in the underlying silicon substrate. The presence of these defects not only creates imperfections in the oxide, but also causes non-uniformity in the distribution of the electric field applied to the sample [19]. Non-uniform dopant distribution will modify the interpretation of the measurements of interface trap properties, and the change of the surface concentration will affect the threshold voltage and device contact resistance [19].

The simulated values in Fig. 14 also showed a slight downward trend, as opposed to those found from measurement. The difference in the slopes of the two traces is explained as follows. The simulated values follow that of theory as expected, since dielectrics become more lossy at high frequencies due to the polarization effect. Hence the response exhibits a decreasing slope. The measured values however increase slightly with frequency, but they agree quite well with simulation within the bandwidth of the $\lambda/4$ transformer. Since matching is only optimum when the transformer thickness is $\lambda/4$ however, the bandwidth over which matching occurs is therefore

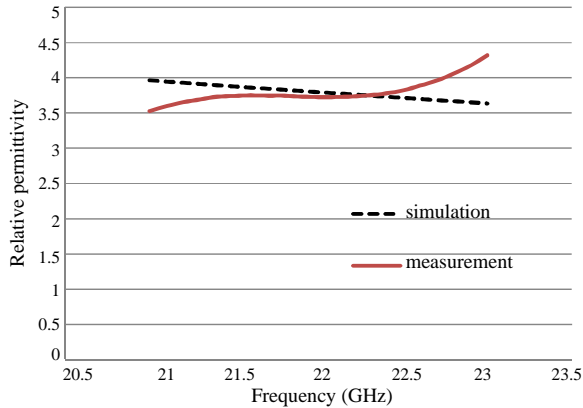


Figure 14. Comparison between simulated and measured ϵ_r of SiO_2 layers grown on p-type Si.

small. Outside this bandwidth, mismatch will set-up reflections, which in turn gives rise to measurement errors. As the frequency increases, the reflections become more severe since the wavelength gets smaller, and thus the difference between measurement and simulation increases, yielding an upward trend for the measured values as shown. Improved accuracies should be possible if transformers offering wider bandwidths such as multi-section quarter-wave transformers are used, but employing these types of transformers would complicate the system since the analysis would have to include the effects of these various sections in de-embedding the S parameters of the samples.

4.2.2. Variation with Oxide Layer Thickness

The effect of layer thickness on the relative permittivity values was also investigated. In this work, the oxidation process used for oxide growth was wet oxidation at 1000°C . The oxide furnace was first heated to 200°C , with N_2 gas flowing to the chamber. When the temperature rose to 200°C , a quartz wafer boat was inserted into the furnace using a quartz rod. The Si wafers were placed on the quartz boat.

Once the furnace temperature rose to 1000°C , the N_2 was changed with O_2 . During this period the wafer is oxidized, and the time the wafers are subjected to O_2 determines the thickness of the oxide layer. A $1\ \mu\text{m}$ thick oxide layer typically requires $4\frac{1}{2}$ hours of oxidation. The oxygen flowed through a bubbler that contains boiling water which will then carry water vapor to the oxidation chamber. After the desired time elapsed, the O_2 flow was disabled, while N_2 flow continues during

ramp down. At approximately 500°C, the N_2 flow was disabled and the wafers were left overnight for cooling down to room temperature before being taken out.

In this work, the oxide film thickness was determined using *Filmetrics F20*, a general purpose film thickness measurement instrument. The instrument uses a technique called spectral reflectance, where the film thickness is measured by reflecting light off the film and analyzing the reflected light over a range of wavelengths. The instrument can measure film thicknesses from 3 nm up to 1 mm.

Oxide layers of four different thicknesses, namely 0.1, 0.2, 0.5 and 0.9 μm , were grown on p-type Si substrates. Fig. 15 shows the measured results, while Table 2 shows $|S_{11}|$ of all samples at 22 GHz.

From the graph, it is clear that there is a significant difference in $|S_{11}|$ for samples with different oxide thicknesses. The $|S_{11}|$ values decrease with increasing oxide thickness, implying that less signals were reflected as the oxide becomes thicker. As the oxide layer gets thicker however, the reduction of $|S_{11}|$ becomes less. This could be caused by charged trapping and skin effect and is discussed as follows.

The difference in $|S_{11}|$ response for different oxide thicknesses can be explained by the phenomenon of charge carrier trapping. Trapping is caused by defects in the crystal which lead to temporary removal of

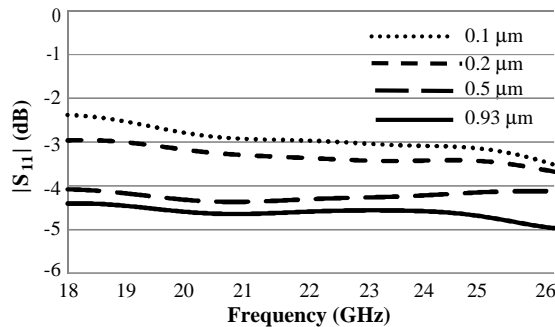


Figure 15. $|S_{11}|$ for different oxide layer thicknesses.

Table 2. $|S_{11}|$ of different oxide thicknesses at 22 GHz.

Oxide Thickness (μm)	$ S_{11} $
0.1	0.71
0.2	0.68
0.5	0.61
0.9	0.59

the electron from the conduction band [12]. There are four general types of charges associated with the SiO₂-Si system, namely fixed oxide charge, mobile oxide charge, trapped oxide charge, and trapped interface charge.

The interface trapped charges are positive or negative charges, created due to structural defects, oxidation-induced defects, metal impurities, or other defects caused by radiation or similar bond-breaking processes [20]. These trapped charges are located at the Si-SiO₂ interface, whereby their concentration increased with the oxide thickness [21]. This could be explained by the fact that more holes were attracted towards the Si/SiO₂ interface as the oxide thickness decreases. The inversion holes weaken the Si-H bonds, leading to the creation of more trapped charges [22, 23].

When RF signals are applied to the sample, the high operating frequency resulted in the period of the applied signal to become comparable to the time constant of the trapping and de-trapping of the interface states. Kwan and Deen [24] found in their measurements that carrier trapping affected *S*-parameter measurements, whereby the $|S_{11}|$ increased with increasing interface traps. They also reported that electron mobility decreases with increasing interface traps. Based on these arguments, it can be proposed that interface traps exist more in thinner oxides where it reduces the electron mobility, hence decreasing the conductivity. This supports the notion that $|S_{11}|$ increases with decreasing oxide thickness as the result of charge trapping.

The effect of oxide layer thickness on S_{11} response may be discussed further based on surface potential, which is generated by a difference in the work function of the materials used. Nevin and Chamberlain [25] studied the effect of oxide thickness on the properties of metal-insulator-semiconductor device and found that the surface potential of the device is lowered with thicker oxide layers. As the layer gets thicker, the surface potential decreases, reducing the field strength in the process.

The change in $|S_{11}|$ is directly related to changes in the surface potential which result from the field associated with the charges of the layer. The reflection coefficient $|S_{11}|$ is proportional to the ratio of the incident electric field E_o to the reflected field E_r ;

$$|S_{11}| \propto \frac{E_r}{E_o} \quad (20)$$

When the oxide layer gets thicker, the surface potential reduces and this lowers the electric field associated with it. From (20) we see that, for the same electric field incident on the samples, as the oxide thickness is increased, the reflected field is thus reduced, and this leads to a reduction in $|S_{11}|$.

The effect of oxide thickness can be further discussed by the loss tangent, $\tan \delta$, which is a measure of the energy loss due to microwave absorption within the material. The loss tangent is the ratio of ε'' to ε' , and is also related to the oxide thickness as follows [26]:

$$\tan \delta = \frac{\varepsilon''}{\varepsilon'} = \frac{1}{2} \left(\frac{ed}{2} \right)^{1/2} \left(\frac{n\varepsilon_o}{2\pi\varepsilon_\infty kT} \right)^{1/4} \quad (21)$$

where d is the oxide thickness, k is the Boltzmann's constant, ε_∞ the radio frequency relative permittivity, and T the temperature. The carrier density n is independent of thickness, while $\tan \delta$ varies with $d^{1/2}$. It can be shown further that $\tan \delta$ depends on the conductivity through the relation [26]

$$\varepsilon'' = \frac{\sigma}{\omega} \quad (22)$$

From (21) we see that as the oxide layer gets thinner, $\tan \delta$ decreases, and from (22), the conductivity decreases in the process, leading to an increase in $|S_{11}|$ as seen in the experiment.

Ismail et al. [27] studied the reflection characteristics of dielectric substrates having a variety of relative permittivity and loss tangent values, and reported that samples with higher ε and loss tangent absorb more incident signal. This was explained by the fact that the increasing ε and loss tangent causes more multiple reflections in the dielectric, thus dissipating more energy in the dielectric [27]. This leads to degradation in the reflectivity of the dielectric, which concurs with the behavior we see with our samples in this experiment.

4.2.3. Skin Effect

At microwave frequencies, the penetration of currents and magnetic fields into the surface of a material is governed by skin effect. Skin effect is the tendency for high frequency alternating currents and magnetic flux to penetrate into the surface of a conductor only to a limited depth [28]. Skin effect, δ , also termed as 'depth of penetration', depends on the frequency, f , the conductivity, σ , and the permeability of the material, μ . If the thickness of a material is much greater than the depth of penetration, its behavior toward high frequency alternating currents becomes a surface phenomenon rather than a volume phenomenon [28].

In this experiment, the conductivity of the SiO₂ was deduced from the electromagnetic simulation through optimization. For a conductivity value of 60 S/m, the calculated skin effect is 0.5 μm . It can be seen from Table 1 that as the oxide thickness becomes greater than 0.5 μm , the S_{11} reduction becomes less compared to the reduction

seen in the range 0.1 to 0.5 μm . This seems to imply that as the oxide layer gets thicker than the skin depth, more RF signals are confined in the skin depth, and thus the reflection which resulted is more due to the surface, rather than bulk, phenomenon. This result also shows that the measurement technique is reliable because it is sensitive to the properties of the epitaxial layer only. The presence of the substrate, whose conductivity is several orders of magnitude larger than the layer to be measured, did not seem to affect the data measured [29].

5. CONCLUSIONS

A non-destructive, non-contact technique for measuring the complex permittivity of double-layer bulk dielectric and thin film dielectric at microwave frequencies has been developed. The set up consisted of spot-focusing horn antennas and a vector network analyzer for measuring the reflected signals. Two methods were used in the experiments — Metal-Backed Method for thin film dielectric, and Transmission Method and Metal-Backed Method for bulk dielectrics. The quarter-wave transformers used improved the matching at the middle of the frequency band.

The permittivity values found for both bulk and thin film dielectrics compared favourably to those reported in literature. The values found for PVC and Plexiglas differ from published data by less than 1%, while those of SiO_2 agreed to within 2% of the reported figures. More importantly, the method allows accurate characterization of the epitaxial layers of a semiconductor wafer by being able to isolate the effect of the underlying substrate provided the film thicknesses were less than the skin depth. These results show the important contribution of this work in characterizing thin films at microwave frequencies. The fact that the method is both non-contacting and non-destructive leads to the reduction of errors due to contact resistance and parasitics, both of which are normally significant at high frequencies.

ACKNOWLEDGMENT

The authors would like to acknowledge Universiti Teknologi MARA for funding this work under the *Dana Kecemerlangan* research fund.

REFERENCES

1. Hambley, A. R., *Electronics*, 2nd edition, Prentice-Hall International, Inc., New Jersey, 2000.

2. Ahmad, S., *Microwave and Millimeter Wave Semiconductor Materials Technology*, Tata McGraw-Hill, New York, 1998.
3. Baba, N. H., Z. Awang, and D. K. Ghodgaonkar, "Accuracy considerations for dielectric measurements of semiconductor wafers using free space microwave measurement system in 8–13 GHz range," *Proc. IEEE Int. RF and Microwave Conf. (RFM)*, 177–181, Kuala Lumpur, Oct. 5–6, 2004.
4. Saad, T. S., R. C. Hansen, and G. J. Wheeler, *Microwave Engineers' Handbook*, Vol. 1., 179, Artech House, Boston, 1971.
5. Ghodgaonkar, D. K., V. V. Varadan, and V. K. Varadan, "Free-space measurement of complex permittivity and complex permeability of magnetic materials at microwave frequencies," *IEEE Trans. of Inst. and Measurement*, Vol. 39, No. 2, 387–394, Apr. 1990.
6. Srivastava, G. P. and V. L. Gupta, *Microwave Devices and Circuit Design*, Prentice-Hall India, New Delhi, 2006.
7. Ghodgaonkar, D. K., V. V. Varadan, and V. K. Varadan, "A free-space method for measurement of dielectric constants and loss tangents at microwave frequencies," *IEEE Trans. of Inst. and Measurement*, Vol. 38, No. 3, 789–793, Jun. 1989.
8. Baba, N. H., *Microwave Non-destructive Testing of Semiconductor Materials*, M.Sc. thesis, Universiti Teknologi MARA, Apr. 2005.
9. Millitech, Inc., Series GOA Gaussian Optics Lens Antenna.
10. Hippel, A. V., *Dielectric Materials and Applications*, Artech House, Boston, 1995.
11. Zant, P. V., *Microchip Fabrication*, 5th Edition, McGraw-Hill, New York, 2004.
12. Kasap, S. O., *Principles of Electronic Materials and Devices*, 2nd Edition, McGraw-Hill, New York, 2002.
13. Kawate, E. and B. Prijamboedi, "Development of the measurement method of dielectric constant of low-k film in the millimeter wave region," *Proc. Joint 29th Int. Conf. on Infrared and Millimeter Waves and 12th Int. Conf. on Terahertz Electronics*, 801–802, Karlsruhe, Germany, Oct. 2004.
14. Bakker, G. L. and D. W. Hess, "Removal of thermally grown SiO₂ films using water at elevated temperature and pressure," *Electrochem. Soc. Proc.*, Vol. 95–20, 464–471, 1996.
15. Harper, C. A., *Handbook of Ceramics, Glasses and Diamonds*, McGraw-Hill, New York, 2001.
16. Baker-Jarvis, J., et al., "Dielectric characterization of low-loss materials: A comparison technique," *IEEE Trans. Dielectric Elect.*

- Ins.*, Vol. 5, No. 4, 571–577, Aug. 1998.
17. Albertin, K. F., M. A. Valle, and I. Pereyra, “Study of MOS capacitors with TiO₂ and SiO₂/TiO₂ gate dielectric,” *J. Int. Cir. Systems*, Vol. 2, 89–93, 2007.
 18. Shackelford, J. F., W. Alexander, and J. S. Park, *Materials Science and Engineering*, 2nd Edition, CRC Press, Inc., Boca Raton, 1994.
 19. May, G. S. and S. M. Sze, *Fundamentals of Semiconductor Fabrication*, John Wiley and Sons, New York, 2004.
 20. Schroder, D. K., *Semiconductor Material and Device Characterization*, 2nd Edition, John Wiley & Sons, Inc., New York, 2004.
 21. Hadi, D. A., S. F. W. M. Hatta, and N. Soin, “Effect of oxide thickness on 32 nm PMOSFET reliability,” *Proc. IEEE Int. Conf. on Semicond. Electron. (ICSE)*, 244–247, Jun. 28–30, 2010.
 22. Mahapatra, S., M. A. Alam, P. B. Kumar, T. R. Dalei, D. Varghese, and D. Saha, “Negative bias temperature instability in CMOS devices,” *Microelectronics Eng.*, Vol. 80, 114–121, 2005.
 23. Alam, M. A., H. Kufluoglu, D. Varghese, and S. Mahapatra, “A comprehensive model for PMOS NBTI degradation: Recent progress,” *Microelectronics Rel.*, Vol. 47, 853–862, Dec. 2006.
 24. Kwan, W. S. and M. J. Deen, “Hot-carrier effects on the scattering parameters of lightly doped drain n-type metal-oxide-semiconductor field effect transistor,” *J. Vac. Sci. Technol.*, Vol. 16, No. 2, 628–632, Jan. 1998.
 25. Nevin, W. A. and G. A. Chamberlain, “Effect of oxide thickness on the properties of metal-insulator-organic semiconductor photovoltaic cells,” *IEEE Trans. on Electron. Devices*, Vol. 40, No. 1, 75–81, Jan. 1993.
 26. Burkhardt, P. J., “Dielectric relaxation in thermally grown SiO₂ films,” *IEEE Trans. on Elect. Dev.*, Vol. 13, No. 2, 268–275, Feb. 1966.
 27. Ismail, M. Y., M. Inam, and A. M. A. Zaidi, “Reflectivity of reflectarrays based on dielectric substrates,” *Amer. J. of Eng. Appl. Sci.*, Vol. 3, No. 1, 180–185, 2010.
 28. Wheeler, H. A., “Formulas for the skin effect,” *Proc. of the IRE*, Vol. 30, No. 9, 412–424, Sept. 1942.
 29. Bichara, M. R. E. and J. P. R. Poitevin, “Resistivity measurement of semiconducting epitaxial layers by the reflection of a hyperfrequency electromagnetic wave,” *IEEE Trans. Inst. Meas.*, Vol. 13, 323–328, Dec. 1964.